IEEE Photonics Journal
An IEEE Photonics Society Publication

Open Access

Design of a Broadband and Low Loss TM Magneto-Optical Waveguide Isolator Based on Lithium Niobate on Insulator

Volume 13, Number 2, April 2021

Mingxuan Li
Yiru Zhao
Shuangxing Dai
Wenqi Yu
Jinye Li
Zhike Zhang
Jianguo Liu, ***Member, IEEE***

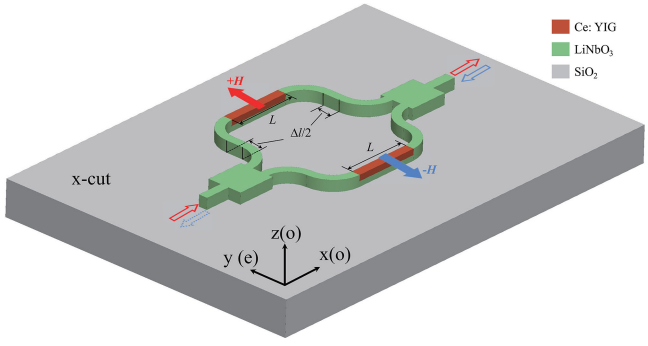

DOI: 10.1109/JPHOT.2021.3058686

Design of a Broadband and Low Loss TM Magneto-Optical Waveguide Isolator Based on Lithium Niobate on Insulator

Mingxuan Li,[1,2] **Yiru Zhao**,[1,2] **Shuangxing Dai**,[1,2] **Wenqi Yu**,[1,2] **Jinye Li**,[1] **Zhike Zhang**,[1] **and Jianguo Liu**,[1,2] ***Member, IEEE***

[1]State Key Laboratory on Integrated Optoelectronics, Institute of Semiconductors, Chinese Academy of Sciences, Beijing 100083, China
[2]College of Materials Science and Opto-Electronic Technology, University of Chinese Academy of Sciences, Beijing 100049, China

DOI:10.1109/JPHOT.2021.3058686

Manuscript received October 27, 2020; revised February 4, 2021; accepted February 8, 2021. Date of publication February 11, 2021; date of current version March 10, 2021. This work was supported in part by the National Natural Science Foundation of China (NSFC, NO. 11674313, 61535014, 61527820, 61674142, 62041502) and in part by the National Key R&D Program of China (No. 2019YFB2203700, 2018YFB2200504). Corresponding author: Jianguo Liu (e-mail: jgliu@semi.ac.cn).

Abstract: We proposed a design of a fundamental TM mode waveguide optical isolator using lithium niobate on insulator (LNOI) and deposited magneto-optical film. The optical isolator adopts an asymmetric Mach-Zehnder interferometer (MZI) structure composed of two 1 $\times$ 2 MMIs, non-reciprocal and reciprocal waveguides. We used three methods to calculate the non-reciprocal phase shift (NRPS) of the lithium niobate (LN)/ Ce: YIG composite waveguide and got similar results. The device shows about 51.98 nm 30 dB isolation bandwidth and 1.20 dB simulated insertion loss at the wavelength of 1550 nm. The fabrication tolerances and a suitable process are also discussed to meet the state-of-art technology and material properties.

Index Terms: Optical isolator, nonreciprocal phase shift, magneto-optical, Mach-Zehnder interferometer, lithium niobate on insulator.

1. Introduction

In optical communication systems, non-reciprocal optical devices, such as optical isolators and optical circulators, control the unidirectional transmission of light in waveguides or optical fibers. In particular, optical isolators are widely used to block the reflected light and protect the active devices such as lasers and amplifiers [1], [2].

In recent years, on-chip platforms of various material systems have emerged, such as silicon carbide (SiC) [3]/silicon oxycarbide (SiOC) [4]/silicon nitride (SiN) [5]/silicon on insulator (SOI) [6], [7], PLC [8], lithium niobate (LN)/lithium niobate on insulator (LNOI) [9], [10], etc. The integrated optical isolators on these platforms will play an irreplaceable role in ensuring the function of photonic integrated systems.

At present, many methods have been tried to realize integrated optical isolators. In the earliest, Wolfe *et al.* realized a Faraday rotation isolator by etching triple-layer bismuth yttrium iron garnet (Bi: YIG) film on gadolinium gallium garnet (GGG) substrates [11]. Isolation ratios of $\sim$25 dB or better were achieved over a wavelength range of $\pm$ 0.03 μm near 1.5 μm. Later, N. Sugimoto *et al.* realized an isolator with insertion loss lower than 3.2 dB and isolation over 25 dB in the 1.5 μm

wavelength band, which was integrated on PLC platform [12]. However, effective Faraday rotation only exists in square waveguides, while in rectangular waveguides complete energy conversion is prevented by the mismatch in propagation constants between TE and TM modes due to the shape-induced birefringence [13]. With the discovery of new garnet with larger magneto-optic coefficients [14] and the application of Mach-Zehnder interferometer (MZI) [15]–[17], researchers designed isolators available for rectangular waveguides and with smaller footprints. Yokoi *et al.* firstly presented the calculation of non-reciprocal phase shift (NRPS) in magneto-optical (MO)-Si layer and proposed using direct bonding technique to integrate MO layer onto Si waveguides [18]. Then in 2008, device was realized for the first time on SOI platform by Y. Shoji using this method [19]. It showed an isolation ratio of 21 dB and an insertion loss of 8 dB at the wavelength of 1559 nm. The total length of the isolator was 4.0 mm, which was the 50% length of device in [2]. Later, to obtain high quality MO layers on SOI, researchers using other methods such as benzocyclobutene (BCB) adhesive bonding [20], [21], pulsed laser deposition [22]–[25] etc. The latest device was fabricated by Yan Zhang *et al.* [25]. With a device footprint of 0.94 mm $\times$ 0.33 mm, the isolator reached a maximum isolation ratio of 30 dB at the wavelength of 1574.5 nm and an $\sim$5 dB insertion loss. These devices mostly adopted the structure of radiative-coupled magneto-optical waveguides. When coupling with magneto-optical waveguides, the mismatches in size and effective refractive indices will bring extra loss, so specific coupling structure design is needed to reduce the loss.

Recently, devices and optical systems on LNOI are booming, because LN offers excellent electro-optic, acousto-optic, nonlinear effects as well as low loss at the communication band [26]–[28]. The latest research shows that the waveguide loss of LNOI can be reduced to 0.0029 dB/cm by the state-of-the-art fabrication technology [29]. Besides, LN is easier to form active material than Si by doping with rare earth ions [30]. Hence, compared with SOI, LNOI is the most powerful competitor and is expected to be the best platform in terms of monolithic integrated optical system in the future.

In this paper, we proposed an optical isolator for fundamental TM mode on LNOI platform. The optical isolator adopts asymmetric MZI structure composed of two 1 $\times$ 2 multimode interferometers (MMIs), non-reciprocal and reciprocal waveguides. The LN/ Ce: YIG composite waveguide is used to realize the non-reciprocal waveguide. Then we used three methods to calculate the NRPS of LN/ Ce: YIG composite waveguides with different geometries and get similar results. The shortest nonreciprocal waveguide length is obtained while the NRPS is up to a maximum of 4730.28 rad/m. When the length difference between LN waveguides is 0.224 μm, the 30 dB isolation bandwidth is greater than 51.98 nm and the simulated insertion loss is 1.20 dB at the center wavelength of 1550 nm. In addition, we analyzed the influences of device geometries on isolation bandwidth and fabrication tolerances. And we also conceived a reasonable process flow suitable for the device.

2. Theory and Device Design

2.1 Isolation Using NRPS

When an MO material is magnetized in the y direction, its dielectric constant tensor has the following form [27]:

$$\varepsilon = \begin{pmatrix} \varepsilon_{xx} & 0 & -j\gamma \\ 0 & \varepsilon_{yy} & 0 \\ j\gamma & 0 & \varepsilon_{zz} \end{pmatrix} \tag{1}$$

γ is the off-diagonal term of the dielectric constant tensor, which is determined by Faraday rotation θ_F as $\gamma = 2n\theta_F/k_0$, where k_0 is the wave number in vacuum and n is the refractive index.

As shown in Fig. 1, when the light propagates along x axis in MO waveguide, it will show different propagation constants (β_1, β_2) in the opposite two directions. Here, β_1 and β_2 means the propagation constants in MO waveguides with opposite propagating directions or with opposite magnetized directions. β_0 means the propagation constant in other reciprocal materials, such as air, LN etc. ω is the frequency of light. H with arrow means the magnetization direction. That is the non-reciprocal phase shift (NRPS) phenomena. NRPS is defined as the difference between two

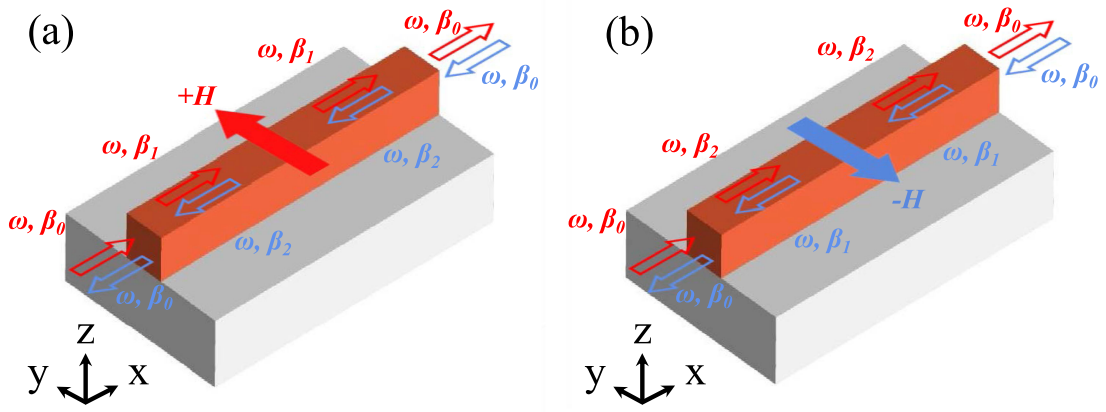

Fig. 1. Propagation constants in opposite directions in MO waveguides when (a) MO is magnetized in the +y direction; (b) MO is magnetized in the -y direction.

propagation constants:

$$\mathrm{NRPS} = \Delta\beta = \beta_1 - \beta_2 \tag{2}$$

The relationship between NRPS and dielectric constant tensor of MO can be obtained by introducing dielectric constant tensor ε into Maxwell equations as follows:

$$\Delta\beta_{TM} = \frac{2\beta_{TM}}{\omega\varepsilon_0 N}\iint \frac{\gamma}{{n_0}^4} H_y \partial_z H_y dydz \tag{3}$$

Where N is the normalized power flow density. According to the (3), for a given material, the NRPS of TM mode light propagating in +x and -x directions is determined by the integration of Hy in y-o-z waveguide section.

Our isolator is an asymmetric Mach-Zehnder interferometer (MZI). The upper arm comprises an MO waveguide with length L and a LN waveguide with length $L' + \Delta l$. The lower arm consists of an MO waveguide with length L and a LN waveguide with length L'. Two MO waveguides have opposite magnetization, in order to generate different propagation constants in two arms. Fig. 2 (a)–(b) shows how the forward and backward light propagate in the isolator and the working principle of isolation. Because of the length asymmetry of LN waveguides and the difference of propagation constants of MO waveguides, light in two arms will get different phases. Each end of the arm is connected to a 3dB coupler, so that the two arms would interfere constructively in the forward direction, and destructively in the backward direction.

If the propagation constant of light in LN waveguide is β_0, according to $\varphi = \beta L$, the additional phase of forward light in the upper arm is $\varphi_{upper+} = \beta_0(L' + \Delta l) + \beta_1 L$, while the that in the lower arm is $\varphi_{lower+} = \beta_0 L' + \beta_2 L$. For the backward light they are $\varphi_{upper-} = \beta_0(L' + \Delta l) + \beta_2 L$ in the upper arm and $\varphi_{lower-} = \beta_0 L' + \beta_1 L$ in the lower arm. In order to satisfy the constructive interference condition in forward direction, the phase difference should be $\Delta\varphi_+ = \varphi_{upper+} - \varphi_{lower+} = 2m\pi$. Similarly, to satisfy the destructive interference condition in backward direction, the phase difference should be $\Delta\varphi_- = \varphi_{upper-} - \varphi_{lower-} = (2n+1)\pi$, where m and n are integers. Combine two equations we can get:

$$\Delta l = \frac{(2m + 2n + 1)\,\pi}{2\beta_0} \tag{4}$$

$$L = \frac{(2m - 2n - 1)\,\pi}{2\,(\beta_1 - \beta_2)} = \frac{(2m - 2n - 1)\,\pi}{2\mathrm{NRPS}} \tag{5}$$

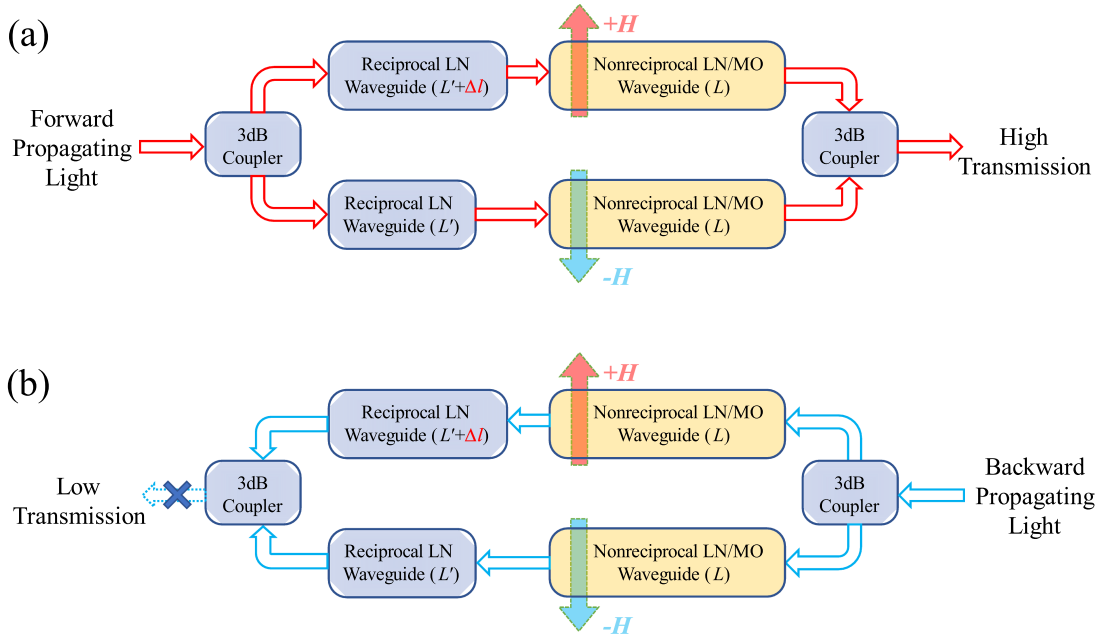

Fig. 2. Operating principle of MZI type magneto-optical isolator on LNOI. (a) Forward propagation; (b) backward propagation.

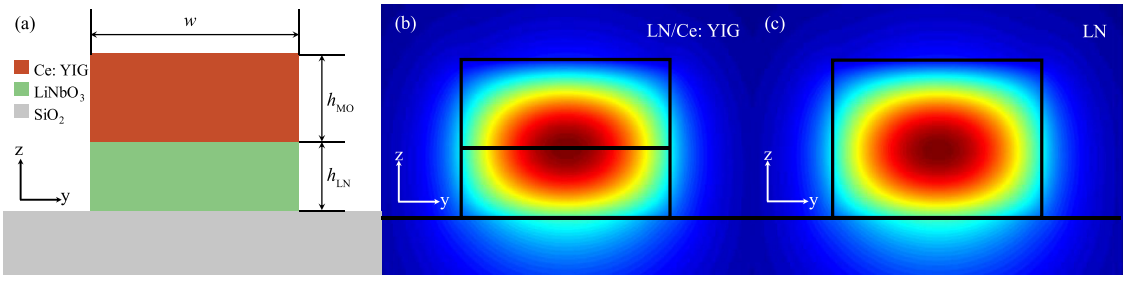

Fig. 3. Cross-section and mode field distribution of waveguides. (a) Structure of non-reciprocal waveguide composed of LN/ Ce: YIG; (b) Hy distribution of non-reciprocal waveguide; (c) Hy distribution of reciprocal waveguide.

2.2 Non-reciprocal Waveguide Structure

It can be seen from (5) that in order to obtain a shorter device length, it is necessary to obtain a larger NRPS. According to (3), NRPS increases with the increase of the gradient of Hy in the z axis. We chose Ce: YIG as MO material because it has a large Faraday rotation coefficient θ_F and an extremely similar refractive index with LN at the wavelength of around 1550 nm. Thus, we designed the non-reciprocal waveguide composed of LN and Ce: YIG. The mode is similar to that in LN waveguide with the same size, so it will have good coupling efficiency with butt coupling. In order to obtain larger NRPS, we made the lower surface of Ce: YIG be located at the position where Hy is strongest and the upper surface be located at the mode edge. As shown in the Fig. 3, Fig. 3. (a) is a cross-sectional view of the LN/Ce: YIG waveguide, and Fig. 3. (b)–(c) shows Hy distribution of fundamental TM mode in the LN/Ce: YIG waveguide and LN waveguide with the same size, respectively.

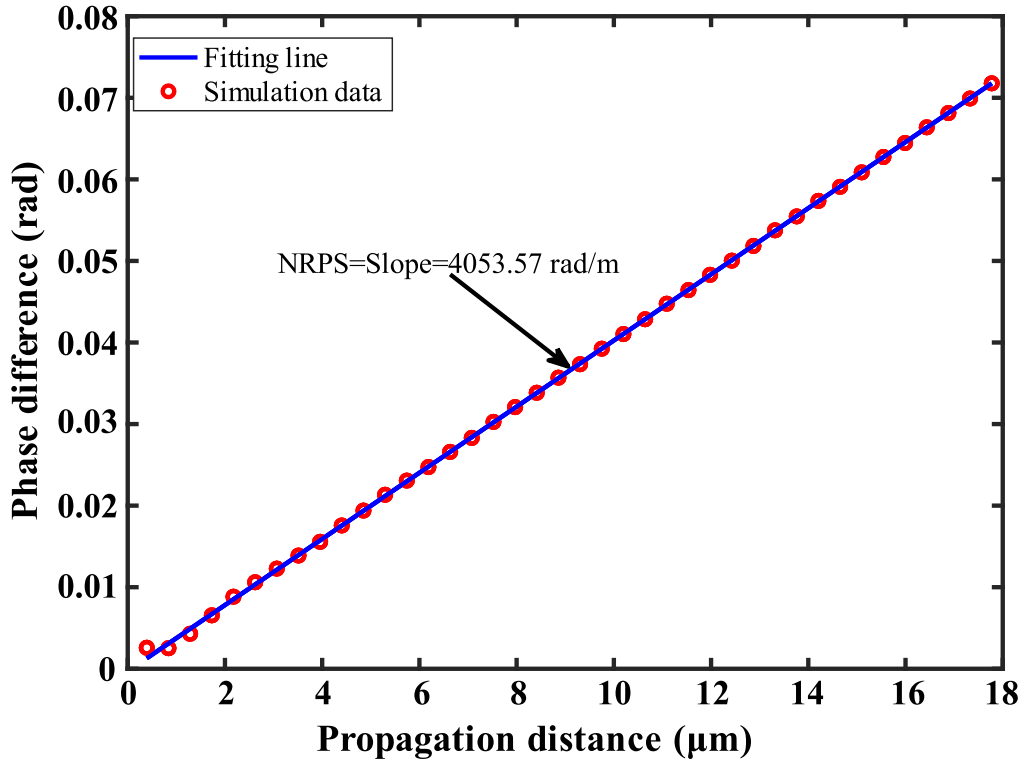

Fig. 4. Phase difference of Hy in opposite propagating directions and linear fitting curve.

3. Results and Discussion

3.1 NRPS Calculation

As can be seen from the previous section, NRPS determines the length of the nonreciprocal waveguide, and also affects the loss and compactness, so solving the magnitude of NRPS is the key to design devices. In this section, we used three simulation methods to calculate the NRPS, and the results are in good consistency. The LNOI wafer we used is x-cut configuration, so the extraordinary axis is the y-axis, and the refractive indices of x, z, y axes are $n_x = n_z = n_o = 2.21$, $n_y = n_e = 2.13$, respectively. Unless otherwise specified, the refractive index of Ce: YIG and SiO_2 are assumed to be 2.22 and 1.444 respectively. The values of Faraday rotation (θ_F) of Ce: YIG films is assumed to be as high as $-4500°$/cm at the wavelength of 1550 nm, which corresponds to a non-diagonal element (γ) of 0.0086 in the permittivity tensor [31]. In addition, it is important to note that the anisotropic materials like MO materials need to be constructed not only by setting its permittivity tensor ε with diagonal and off-diagonal terms, but also by adding a unitary matrix U and a transformation grid attribute based on U [33]. The ε needs to be multiplied by both matrix U and its complex conjugate transpose U^*. That's the key to realize the MO effect on the simulation tool.

Method 1: We use the finite difference time domain (FDTD) method to calculate the time domain transmission of TM mode light of the wavelength of 1550 nm in the nonreciprocal waveguide. We extracted the phases of the Hy along the forward and backward propagating directions, worked out the phase difference between them and divided it by length, so as to obtain the phase difference of Hy per unit length, which is NRPS. Fig. 4 shows the phase difference data and the fitting line. The red circles are phase difference data subtracted by phases of Hy in forward and backward direction. The blue line is the linear fitting of the simulation data, so NRPS can be obtained by working out the slope.

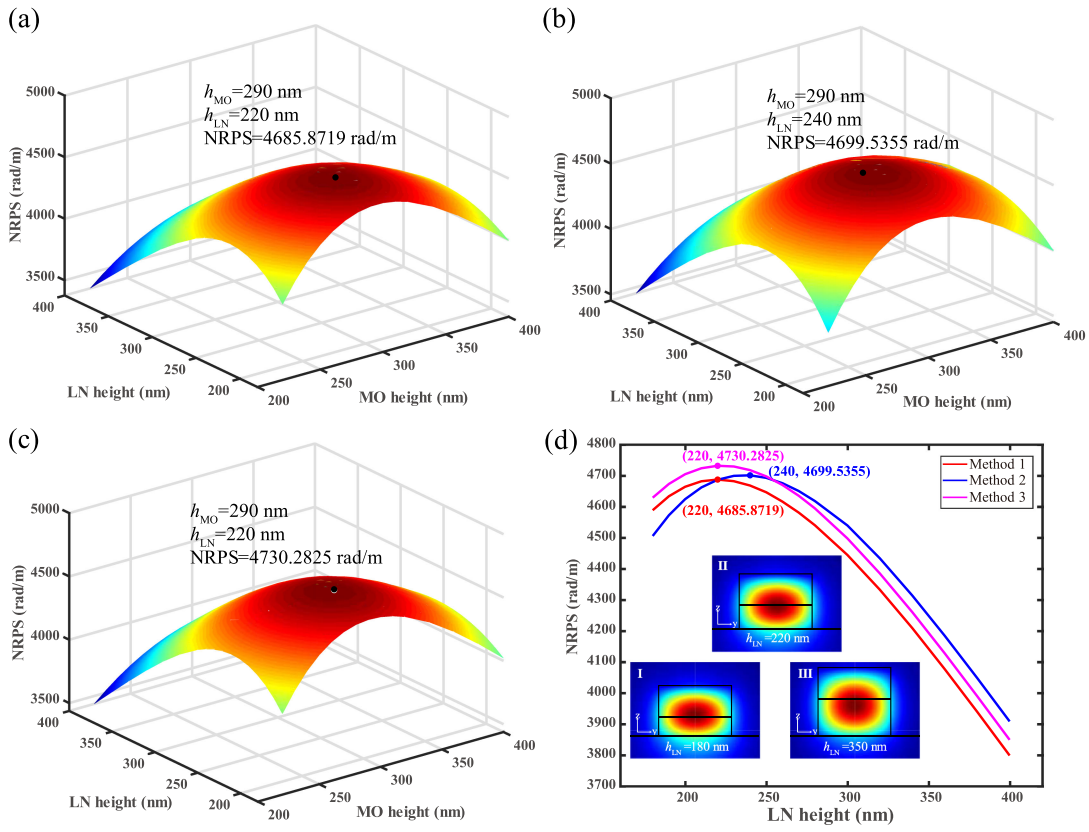

Fig. 5. NRPS with different height combinations of LN/ Ce: YIG waveguide when the waveguide width is w = 900 nm using (a) method 1; (b) method 2; (c) method 3. (d) Comparison of NRPS using 3 methods and the Hy distribution of non-reciprocal waveguide with different height of LN. I-III shows the Hy distribution when h_{LN} is 180 nm, 220 nm, 350 nm respectively.

Method 2: We get the magnetic field distribution in the cross section by solving the mode of the nonreciprocal waveguide, and bring it into the Eq (3) for calculation. This method only needs to solve the mode of waveguide cross-section. However, the results calculated by the formula are greatly influenced by the magnetic field distribution at the interfaces, so it is necessary to accurately extract the magnetic field components at the interfaces. Therefore, it is greatly influenced by the fine degree of grid division.

Method 3: We used the method of solving propagation constants in two opposite directions, and directly get the result of NRPS by calculating the difference between them. The propagation constants were obtained using Finite-Difference Eigenmode (FDE) solver. Due to the small difference between the forward and backward propagation constants, it is also greatly affected by grid division.

Geometric parameters of waveguides will affect the distribution of mode, and then affect NRPS. Therefore, we use three methods to scan non-reciprocal waveguide with different heights and compare them to find the maximum NRPS, as shown in Fig. 5. The NRPS waveguides can satisfy the single mode condition all the time when the width is smaller than 950 nm and the total height is smaller than 540 nm. So we basically refer to this condition to accomplish our simulation.

The figure shows the NRPS of fundamental TM mode with different height combinations of LN/ Ce: YIG waveguide when the waveguide width is $w = 900$ nm. In Fig. 5(a)–(c), we can see that in the above-mentioned height combination, the NRPS obtained by the three methods has a maximum point, and the maximum point of the method 1 and the method 3 is consistent, which appears when $h_{MO} = 290$ nm and $h_{LN} = 220$ nm. The maximum point of method 2 appears at $h_{MO} = 290$ nm and. $h_{LN} = 240$ nm

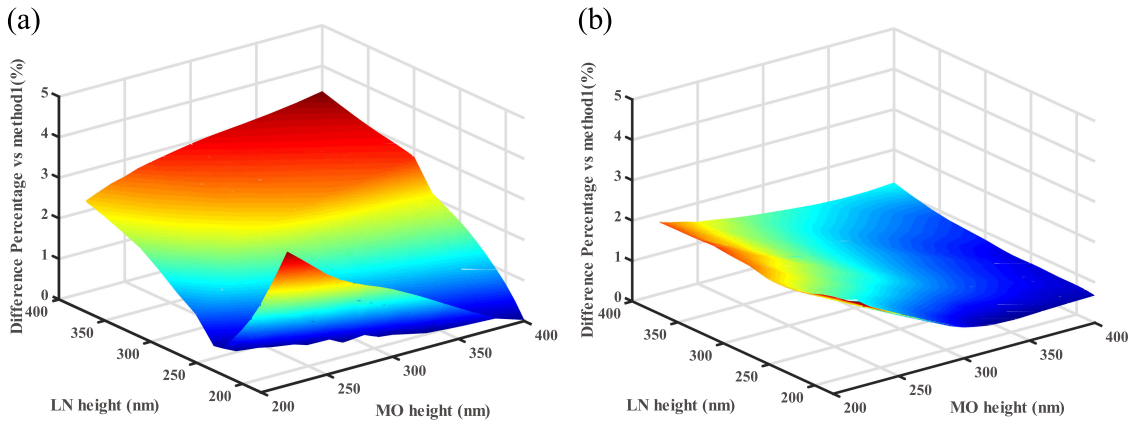

Fig. 6. Difference percentage of NRPS. (a) Method2 versus method1; (b) method 3 versus method1.

It can be seen from (3) that the larger the change rate of Hy on the cross section, the larger the NRPS. By observing the Hy distribution in Fig. 5(d) I-III, it is found that the difference of Hy between the upper and lower interfaces of Ce: YIG increases first and then decreases with the increasing of the height of the nonreciprocal waveguide. The overall trend and numerical value of NRPS obtained by the three methods are basically the same. The main reason of deviation is the calculation method and mechanism of 2D simulation and 3D simulation. Fig. 6 shows that comparing the results calculated by Method 1, the average difference percentage of Method 3 is smaller than that of Method 2, which is due to the simplification and idealization of physical quantities in calculation by formula. All these three methods are reliable, and the closest method to an experiment is 3D-FDTD solution, because it is a direct time and space solution for solving Maxwell's equations in complex geometries. The other two methods are based on FDE solver, which calculates the spatial profile and frequency dependence of modes by solving Maxwell's equations on a cross-sectional mesh of the waveguide. It is a simplified solution to solve the modes distributions on the cross-section of waveguides, but without a solution on the time domain. Thus, for these three methods, method 2 is the simplest one for this kind of problem, method 3 is a mainstream method, and method 1 can be the benchmark.

In addition, we simulated NRPS with different waveguide width using Method 3. The height of LN waveguide is set as $h_{\mathrm{LN}} = 220$ nm, and the height of Ce: YIG is $h_{MO} = 290$ nm. As shown in Fig. 7, when the waveguide width gradually increases from 600 nm to 1500 nm, the NRPS firstly increases then decreases. The reason for choosing 900 nm is to ensure the single-mode condition. When the waveguide width is greater than 1000 nm, high-order TM mode will be excited in the waveguide, which will reduce the content of TM fundamental mode, resulting in smaller NRPS.

3.2 Isolation, Bandwidth and Insertion Loss

According to the results in Section 3.1, we set the geometries of the non-reciprocal waveguide as $h_{LN} = 220$ nm, $h_{MO} = 290$ nm and $w = 900$ nm, so we can obtain the maximum NRPS $=$ 4730.2825 rad/m, and calculate the length of the nonreciprocal waveguide as $L = 324.26\,\mu$m. The geometries of LN reciprocal waveguide is the same as that of non-reciprocal waveguide, with $H = 510$ nm and $w = 900$ nm, then calculate the length difference between upper and lower reciprocal waveguide as $\Delta l = L_0 = 0.224\,\mu$m when $m, n = 0$. Therefore, we have designed fundamental TM mode MO isolator with center wavelength at 1550 nm based on LNOI platform. The device structure is shown in the Fig. 8, and the 3 dB coupler adopts MMI.

Because Δl will affect the working bandwidth of the device, we simulated the transmission of the device with different Δl in the forward and backward direction at the wavelength of

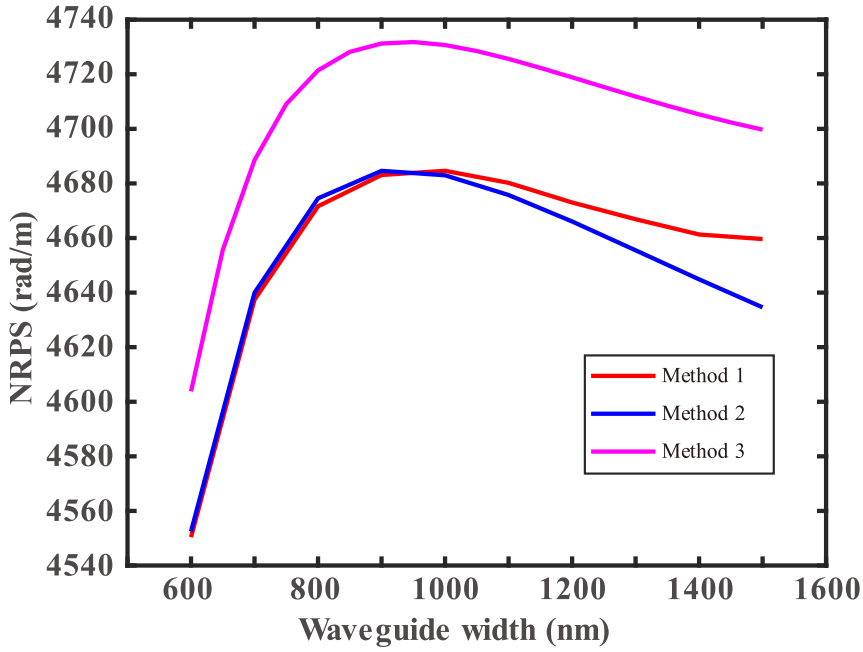

Fig. 7. NRPS with different width of non-reciprocal waveguide when the height of LN waveguide is $h_{LN} = 220$ nm, and the height of Ce: YIG is $h_{MO} = 290$ nm.

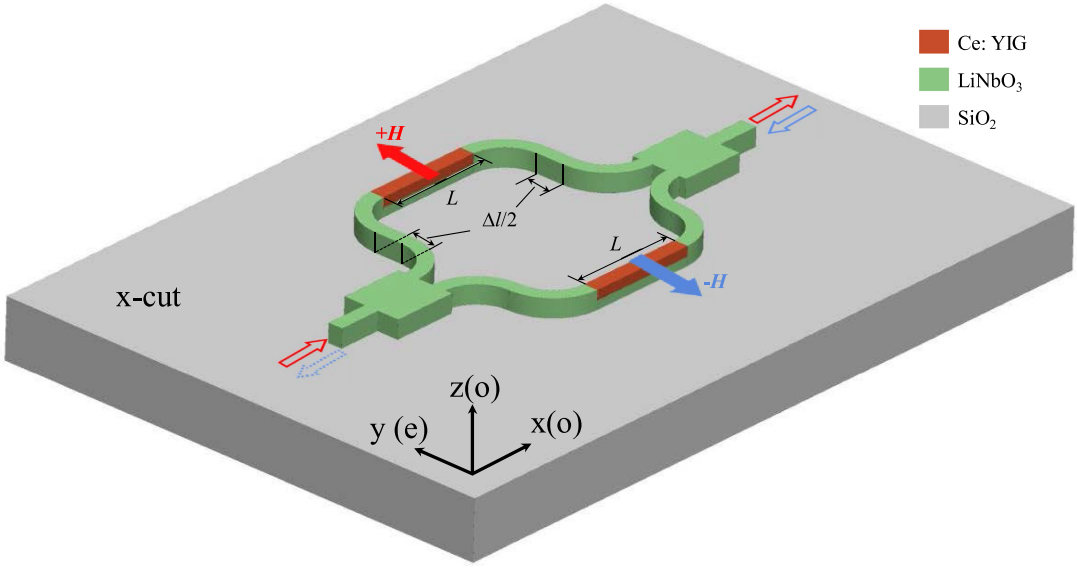

Fig. 8. Sketch of the proposed MZI magneto-optical isolator on LNOI.

1520–1580 nm, shown in Fig. 9. When $m = n = 0, 1, 3, 5$,we obtain $\Delta l = 1L_0, 5L_0, 13L_0, 21L_0$. The red curves in Fig. 9 represent the forward transmittance, and the blue curves represent the backward transmittance. Fig. 9 shows that when $\Delta l = 1L_0$, the 30 dB isolation bandwidth of the device is the maximum, which is 51.98 nm. With the increase of the length difference of reciprocal waveguide, the 30 dB isolation bandwidth gradually decreases.

The insertion loss of the device includes the following aspects: transmission loss of LN waveguide, transmission loss of MO waveguide, butt coupling loss between reciprocal and

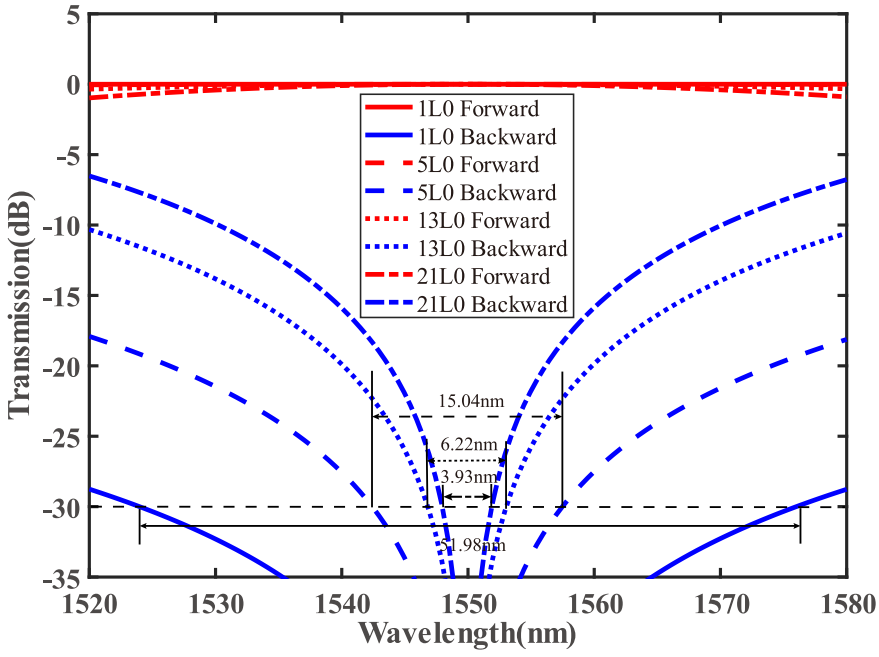

Fig. 9. Transmission of isolator with different Δl in forward and backward propagating directions.

non-reciprocal waveguides, loss of MMI and loss of bent waveguide. Among them, the transmission loss of LN waveguide for light with wavelength of 1550 nm is low enough to ignore. The transmission loss of MO waveguide mainly comes from the absorption loss of the material. According to the literature the absorption loss of Ce: YIG is about 58 dB/cm [33], and the optical confinement factor of Ce: YIG in the composite waveguide is calculated to be 52%, so the transmission loss of MO waveguide is about 0.98dB.

Because the refractive index difference between LN and Ce: YIG is very small near the wavelength of 1550 nm, the modes of light propagating in LN waveguide and the composite waveguide with the same size are almost the same, and the overlapping integral of modes in the two waveguides is over 99.9%, which shows that this structure can realize almost no loss with butt coupling. After optimization, the extra loss of two MMIs can be lower than 0.105dB. The loss of 90° bend waveguide can be reduced by increasing the radius of bend waveguide, which is 0.014 dB when the radius is larger than 30 μm. Therefore, the simulated insertion loss of the device is about 1.20dB.

3.3 Fabrication Design and Tolerance

According to the device structure, we conceived a reasonable fabrication process. As shown in Fig. 10, firstly, Cr mask and electron beam resist were deposited on LNOI wafer, and the pattern of nonreciprocal waveguide was formed by electron beam electron beam lithography (EBL) technology. Then LN trench was etched by RIE technology, and then MO materials were deposited into the trench by magnetron sputtering. Then, the Cr layer and the redundant MO layer are removed by lift-off Cr mask with ceric ammonium nitrate (CAN). Then, the wafer embedded with MO material is overlayed with a bit narrower pattern on MO waveguides by EBL to form the waveguide pattern of the whole device. Finally, the device is fabricated by etching by RIE.

In the process of manufacturing, the fabrication tolerance of waveguide size will have an effect on the propagation constant, which is related to the effect of phase matching and finally affects the isolation bandwidth of the device. So, we calculated the transmissions with different waveguide

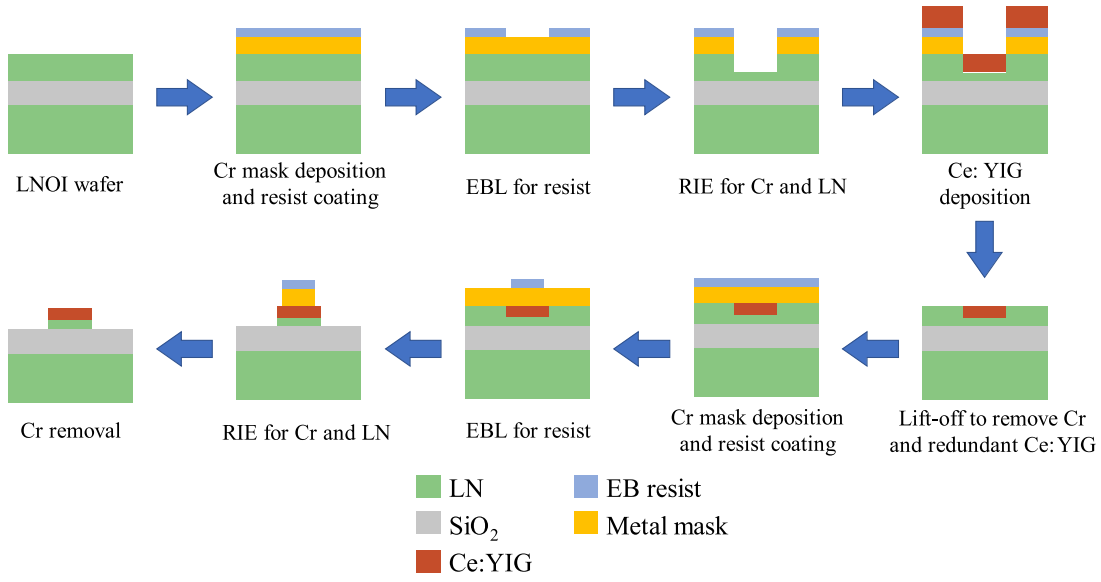

Fig. 10. Design of fabrication process of the device.

length, width and height, in order to see the manufacturing tolerance of the device. To keep the isolation over 30 dB at the wavelength of 1550 nm, the length of the composite waveguide shows a tolerance window of ± 13 μm. The width and the height of the NRPS waveguides show a tolerance window of ± 250 nm and ± 52 nm, respectively. The width, the height and the length of the RPS waveguides show a tolerance window of ± 213 nm, ± 48 nm and ± 8 nm respectively. The fabrication tolerance of the length of RPS waveguides is the smallest. Actually, the common manner to solve this problem is to use large Δl or introduce wavelength-tuning waveguides, just as LN modulators.

4. Conclusion

In summary, we proposed an MZI type TM mode waveguide MO isolator based on LNOI platform. By constructing the LN/Ce: YIG composite structure in the nonreciprocal waveguide region, we observed that when $h_{LN} = 220$ nm, $h_{MO} = 290$ nm and $w = 900$ nm, the structure has the maximum NRPS $= 4730.2825$ rad/m for fundamental TM mode light at wavelength of 1550 nm. When the length of nonreciprocal waveguide is 324.26 μm and the length difference of reciprocal waveguide is 0.224 μm, the device has a 51.98 nm isolation bandwidth of 30 dB near 1550 nm and 1.20 dB simulated insertion loss. The influences of device geometries on isolation bandwidth and fabrication tolerance are analyzed. The reasonable process suitable for the device is also conceived. The device has the advantages of broadband optical isolation and low insertion loss, so it has a good application prospect in LN integrated photonic devices.

Acknowledgment

The authors wish to thank the anonymous reviewers for their valuable suggestions.

References

[1] K. E. Stubkjaer and M. B. Small, "Noise properties of semiconductor-lasers due to optical feedback," *IEEE J Quantum Electron.*, vol. QE-20, no. 5, pp. 472–478, May 1984.
[2] K. Petermann, "External optical feedback phenomena in semiconductor-lasers," *IEEE J. Sel. Topics Quantum Electron.*, vol. 1, no. 2, pp. 480–489, Jun. 1995.

[3] C. Wang, E. Miyazono, I. Craiciu, and A. Faraon, "Hybrid silicon on silicon carbide integrated photonics platform," *Appl. Phys. Lett.*, vol. 115, no. 14, 2019, Art. no. 141105.
[4] F. A. Memon *et al.*, "Silicon oxycarbide platform for integrated photonics," *J. Lightw. Technol.*, vol. 38, no. 4, pp. 784–791, 2020.
[5] X. Hu, M. Girardi, Z. Ye, P. Munoz, A. Larsson, and V. Torres-Company, "$S_{i3}N_4$ photonic integration platform at 1 microm for optical interconnects," *Opt Exp.*, vol. 28, no. 9, pp. 13019–13031, Apr. 2020.
[6] T. Komljenovic *et al.*, "Heterogeneous silicon photonic integrated circuits," *J. Lightw. Technol.*, vol. 34, no. 1, pp. 20–35, 2016.
[7] T. Hu *et al.*, "Silicon photonic platforms for mid-infrared applications," *Photon. Res.*, vol. 5, no. 5, pp. 417–430, 2017.
[8] T. Izuhara *et al.*, "Photonic integrated circuits based on silica and polymer PLC," in *Proc. SPIE OPTO*, San Francisco, CA, USA, Mar. 2013, Art. no. 862807.
[9] I. Krasnokutska, J. J. Tambasco, X. Li, and A. Peruzzo, "Ultra-low loss photonic circuits in lithium niobate on insulator," *Opt Exp.*, vol. 26, no. 2, pp. 897–904, Jan. 2018.
[10] K. Luke, P. Kharel, C. Reimer, L. He, M. Loncar, and M. Zhang, "Wafer-scale low-loss lithium niobate photonic integrated circuits," *Opt. Exp.*, vol. 28, no. 17, pp. 24452–24458, 2020.
[11] R. Wolfe, R. A. Lieberman, V. J. Fratello, R. E. Scotti, and N. Kopylov, "Etch-tuned ridged waveguide magneto-optic isolator," *Appl. Phys. Lett.*, vol. 56, no. 5, pp. 426–428, 1990.
[12] N. Sugimoto *et al.*, "A hybrid integrated waveguide isolator on a silica-based planar lightwave circuit," *J. Lightw. Technol.*, vol. 14, no. 11, pp. 2537–2546, Nov. 1996.
[13] B. J. H. Stadler and T. Mizumoto, "Integrated magneto-optical materials and isolators: A review," *IEEE Photon. J.*, vol. 6, no. 1, Feb. 2014, Art. no. 0600215.
[14] M. Gomi, H. Furuyama, and M. Abe, "Strong magneto-optical enhancement in highly Ce-substituted iron garnet films prepared by sputtering," *J. Appl. Phys.*, vol. 70, no. 11, pp. 7065–7067, 1991.
[15] O. Zhuromskyy, M. Lohmeyer, N. Bahlmann, H. Dotsch, P. Hertel, and A. F. Popkov, "Analysis of polarization independent Mach-Zehnder-type integrated optical isolator," *J. Lightw. Technol.*, vol. 17, no. 7, pp. 1200–1205, Jul. 1999.
[16] N. Bahlmann, M. Lohmeyer, O. Zhuromskyy, H. Dotsch, and P. Hertel, "Nonreciprocal coupled waveguides for integrated optical isolators and circulators for TM modes," *Opt. Commun.*, vol. 161, no. 4–6, pp. 330–337, Mar. 1999.
[17] J. Fujita, M. Levy, R. M. Osgood, L. Wilkens, and H. Dötsch, "Waveguide optical isolator based on Mach–Zehnder interferometer," *Appl. Phys. Lett.*, vol. 76, no. 16, pp. 2158–2160, 2000.
[18] H. Yokoi and T. Mizumoto, "Proposed configuration of integrated optical isolator employing wafer-direct bonding technique," *Electron. Lett.*, vol. 33, no. 21, pp. 1787–1788, Oct. 1997.
[19] Y. Shoji, T. Mizumoto, H. Yokoi, I. W. Hsieh, and R. M. Osgood, "Magneto-optical isolator with silicon waveguides fabricated by direct bonding," *Appl. Phys. Lett.*, vol. 92, no. 7, 2008.
[20] S. Ghosh, S. Keyvavinia, W. Van Roy, T. Mizumoto, G. Roelkens, and R. Baets, "Ce:YIG/Silicon-on-Insulator waveguide optical isolator realized by adhesive bonding," *Opt Exp.*, vol. 20, no. 2, pp. 1839–1848, Jan. 2012.
[21] S. Ghosh, S. Keyvaninia, Y. Shirato, T. Mizumoto, G. Roelkens, and R. Baets, "Optical isolator for TE polarized light realized by adhesive bonding of Ce: YIG on silicon-on-insulator waveguide circuits," *IEEE Photon. J.*, vol. 5, no. 3, Jun. 2013, Art. no. 6601108.
[22] Y. Zhang *et al.*, "Dysprosium substituted Ce:YIG thin films with perpendicular magnetic anisotropy for silicon integrated optical isolator applications," *APL Mater.*, vol. 7, no. 8, 2019, Art. no. 081119.
[23] Y. Zhang *et al.*, "Enhanced magneto-optical effect in $Y_{1.5}Ce_{1.5}Fe_5O_{12}$ thin films deposited on silicon by pulsed laser deposition," *J. Alloys Compounds*, vol. 703, pp. 591–599, 2017.
[24] J. Hu *et al.* "Monolithic on-chip nonreciprocal photonics based on magneto-optical thin films," in *Proc. SPIE 9750, Integr. Opt.: Devices, Materials, and Technologies XX*, San Francisco, CA, USA, Mar. 2016, Art. no. 97500W.
[25] Y. Zhang *et al.*, "Monolithic integration of broadband optical isolators for polarization-diverse silicon photonics," *Optica*, vol. 6, no. 4, pp. 473–478, 2019.
[26] G. D. Boyd, R. C. Miller, K. Nassau, W. L. Bond, and A. Savage, "$LiNbO_3$: An efficient phase matchable nonlinear optical material," *Appl. Phys. Lett.*, vol. 5, no. 11, pp. 234–236, 1964.
[27] G. Poberaj, H. Hu, W. Sohler, and P. Günter, "Lithium niobate on insulator (LNOI) for micro-photonic devices," *Laser Photon. Rev.*, vol. 6, no. 4, pp. 488–503, Jul. 2012.
[28] H. Han, L. Cai, and H. Hu, "Optical and structural properties of single-crystal lithium niobate thin film," *Opt. Mater.*, vol. 42, pp. 47–51, Apr. 2015.
[29] J. Zhou *et al.*, "Electro-Optically switchable optical true delay lines of meter-scale lengths fabricated on lithium niobate on insulator using photolithography assisted chemo-mechanical etching," *Chin. Phys. Lett.*, vol. 37, no. 8, Jul. 2020, Art. no. 084201.
[30] W. Sohler, B. K. Das, D. Dey, S. Reza, H. Suche, and R. Ricken, "Erbium-doped lithium niobate waveguide lasers," *IEICE Trans. Electron.*, vol. E88–C, no. 5, pp. 990–998, 2005.
[31] N. Bahlmann *et al.*, "Improved design of magnetooptic rib waveguides for optical isolators," *J. Lightw. Technol.*, vol. 16, no. 5, pp. 818–823, May 1998.
[32] T. Shintaku, "Integrated optical isolator based on nonreciprocal higher-order mode conversion," *Appl. Phys. Lett.*, vol. 66, no. 21, pp. 2789–2791, 1995.
[33] "Creating anisotropic optical materials in FDTD and MODE," [Online]. Available: https://support.lumerical.com/hc/en-us/articles/360034394694-Creating-anisotropic-optical-materials-in-FDTD-and-MODE
[34] L. Bi *et al.*, "On-chip optical isolation in monolithically integrated non-reciprocal optical resonators," *Nat. Photon.*, vol. 5, no. 12, pp. 758–762, 2011.